Experimental study of creep-damage coupling in concrete by acoustic emission technique

Jacqueline Saliba, Ahmed Loukili, Frédéric Grondin, Jean-Pierre Regoin

Experimental study of creep-damage coupling in concrete by acoustic emission technique

J. Saliba · A. Loukili · F. Grondin · J.-P. Regoin

Abstract In order to design reliable concrete structures, prediction of long term behaviour of concrete is important by considering a coupling between creep and damage. An experimental investigation on the fracture properties of concrete beams submitted to creep bending tests with high levels of sustained load is reported. The influence of creep on the residual capacity and the fracture energy of concrete is studied. The progression of fracture is followed by the measurement of the crack mouth opening displacement during a three-point bending test. The sustained loading seems to increase the flexural strength of concrete, probably because of the consolidation of the hardened cement paste. The acoustic emission (AE) technique is used to perform the characterization of the influence of creep on the crack development. Results give wealth information on the fracture process zone (FPZ) and the propagation of the crack. A decrease in the amplitude distribution of AE hits is observed in the post-peak region for creep specimens. The width of the FPZ also decreases in this later indicating that the material has a more brittle behaviour which may be due to the development of microcracking under creep and the prestressing of the upper zone of the beam.

J. Saliba · A. Loukili (✉) · F. Grondin · J.-P. Regoin
Institut de Recherche en Génie Civil et Mécanique (GeM),
LUNAM Université, UMR-CNRS 6183,
Ecole Centrale de Nantes, Nantes, France
e-mail: ahmed.loukili@ec-nantes.fr

Keywords Acoustic emission technique · Bending creep test · Concrete · Fracture process zone

1 Introduction

Special constructions, such as nuclear power plants, are subjected during their life service to constant load or creep for long period. In these types of constructions, two conditions have to be checked: the strength and the permeability. A low permeability is expected and is respected only if the structure is not cracked. However while creep loading, micro-cracks can appear and conduct by extension to the development of macro-cracks.

The physical origins of the basic creep of concrete are still poorly understood and several theories have been suggested: viscous flow [1], plastic flow [2], seepage of gel water [3], consolidation [4], microprestress of creep sites in cement gel microstructure [5], bond breakage in slip and non linear deformation, and microcracking [6–8]. Creep has important effects on the stresses and deflections of concrete structure. For low load levels, it is assumed that linear viscoelasticity takes place and the instantaneous mechanical behaviour of concrete remains elastic. However, for high load levels, deviation is expected and nonlinear creep occurs [9, 10]. In fact, microcracking may initiate at the moment of load application and begins to grow to form a time-dependent crack path [11, 12]. Special tensile and flexural creep tests on partially-damaged

concrete specimens realized by Carpinteri [13] provide important information on this matter. In this later, concrete is submitted to the interaction between two mechanisms: creep strains and damage (microcracking) initiated by local stresses [14, 15].

Thus cracks grow and interact with the time-dependent response of the bulk material [16] which has an impact on the safety margin and life time of many structures such as containment vessels, cooling towers or dam. Many investigations were performed to study the influence of concrete mixture and other parameters on the cracking mechanisms and the fracture of concrete: strength [17], bond between the matrix and the aggregates [18–20], loading conditions [6, 12, 21], temperature [22], aggregate size [23], boundary conditions and other structural conditions as the size effect. However, none of these studies investigated the effects of creep loading history on the failure mechanisms, including its influence on strength, stiffness, and fracture energy.

This study is part of the project MEFISTO funded by the French National Research Agency (ANR). In this project, we suggest to perform numerical codes for the design of special constructions. Constructors calculate the structure dimensions by applying empirical formulations with a high security factor. In order to improve these calculations, special tests are realized to characterize many parameters according to fracture and creep of concrete. For instance, to design nuclear containments vessels, we have to consider that concrete walls are submitted to creep during their service-life and more particularly to basic creep. The relative humidity is high in the nuclear vessel and the exterior surface of the wall is covered by a waterproofing agent, so no important desiccation occurs in concrete. Complete failure was observed after few days under high sustained loading in desiccation. In this context, it wasn't possible to measure the crack properties. In order to overcome the desiccation effects, basic creep was only considered. The experimental procedure is based on the work of Omar et al. [24]. Concrete beams were submitted to bending creep tests with high level of sustained load (85% of the maximum load). The fracture properties of concrete are then assessed by mechanical tests according to the Rilem recommendations [25].

Before the apparition of the macro-crack and during its propagation, micro-cracks develop in the microstructure. Micro-cracking and damage localization in concrete beams cannot be investigated by the classical measurements. So, as a part of the investigation, the acoustic emission (AE) technique was applied. Crack growth was monitored during the fracture tests in concrete beams before and after creep.

First of all, the materials and the experimental methods are presented. Secondly, the creep and the fracture bending tests are analyzed. Finally, the characterization of crack evolution for aging and creep specimens is suggested by using the AE method.

2 Experimental program

2.1 Material properties

Concrete specimens were mixed with Portland cement CPA-CEMII 42.5, crushed limestone aggregate distributed in fine sand, with a maximum size of 5 mm and a density of 2,570 kg/m^3, and crushed gravel of size 5 to 12.5 mm with a density of 2,620 kg/m^3. A superplasticizer agent (Glenium 27) has been added for the workability. Table 1 shows the mix quantities of constituent materials. This mixture is characterized by a water-to-cement (W/C) ratio of 0.56 and a slump of 70 mm. The proportioning of the cement paste, sand and coarse aggregate were kept constant throughout the program.

The mechanical properties of concrete were determined at 28 days on three $\phi 110 \times 220$ mm^2 cylinders:

–the compressive strength, $f_c = 42.6$ MPa,

–the tensile strength assessed through splitting tests, $f_t = 3.7$ MPa,

–the dynamic elastic modulus determined with a non-destructive method (Grindosonic®), $Edyn = 39$ GPa.

For the flexural test, concrete beams were prepared with the same thickness (b) of 100 mm, depth (h) of 200 mm and length (L) of 800 mm with an effective

Table 1 Concrete mixture proportions

Constituents	Dosage (kg/m^3)
Gravel: G5/12.5 mm	936.0
Sand: 0/5 mm	780.0
Cement: CEMII 42.5	350.0
Water	219.5
Superplasticizer	1.9

span (S) equal to 600 mm. The fresh concrete was poured into beam moulds. A plate vibrator was used to compact the concrete in two layers. Then specimens were covered with a thin sheet of plastic to prevent water loss and were maintained in a climatic chamber at a temperature of 20°C and a relative humidity (RH) of 95%. 24 h after casting, the specimens were stripped off from the moulds and kept for curing in lime water for 28 days, under a temperature condition of 20°C. After 28 days, the specimens were taken out from the curing tanks and a central notch was formed using a diamond saw cut, with a notch-to-depth ratio of 0.2 ($a_0 = h/5$).

2.2 Procedure for the three-point bending test

First of all, the maximum load of concrete beams was measured with the three-point bending test. The fracture test employs a load-controlled universal testing machine as per RILEM-TMC 50 recommendations. Tests were conducted in a 160 kN capacity servohydraulic machine under closed-loop crack mouth opening displacement (CMOD) control. The load was applied with a slow rate of 0.0003 mm/s, such that the peak loads occurred at about 2 min. During each test, load, crosshead displacement and CMOD were measured and recorded up to final failure with a data acquisition system. A general view of the experimental setup is provided in Fig. 1.

Bending creep tests were then performed on frames with a capacity ranging from 5 to 50 kN. The frames were placed in a climate controlled chamber at 50% RH and temperature of 20°C. The load is applied by gravity with a weight and counterweight system, which enables a fine tuning of the load. The displacement was measured at midspan (Fig. 2). Three-point bending creep tests were realized on notched specimens where the exchange of moisture was prevented by a double layer of self-adhesive aluminium paper. Hence basic creep displacement was considered only and was determined by substracting the instantaneous elastic displacement from the total displacement.

Two specimens were loaded in creep at 85% (C85) of the maximum load (F_{max}). In addition, two specimens, cast at the same time, are kept under the same conditions without loading. In the following they will be called “aging specimens”.

After 4 months, aging and creep specimens were submitted to rupture. The AE method was used to follow the crack development in the microstructure during the fracture tests. The AE system comprised of an eight channel AE Win system, a general-purpose interface bus (PCI-DISP4) and a PC for data storage analysis. Four piezoelectric transducers (resonant frequency of 150 kHz) were used. Transducers were placed around the expected location of the Fracture process zone (FPZ) to minimize errors in the AE event localization program [26]. They were placed in a rectangular position (12 × 12 cm^2) on one side of the specimen, with silicon grease as the coupling aging (Fig. 1). The recorded AE amplitudes range from 0 to 100 dB. The detected signals were amplified with a

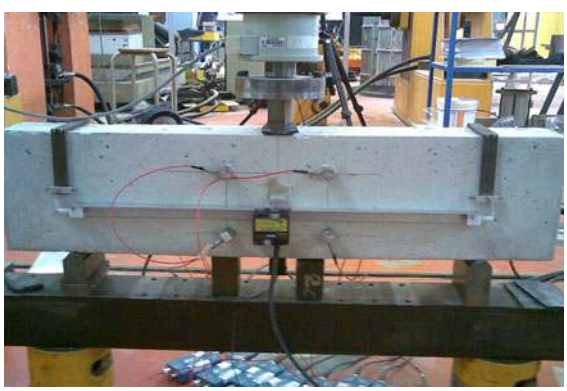

Fig. 1 General view of the experimental fracture test setup

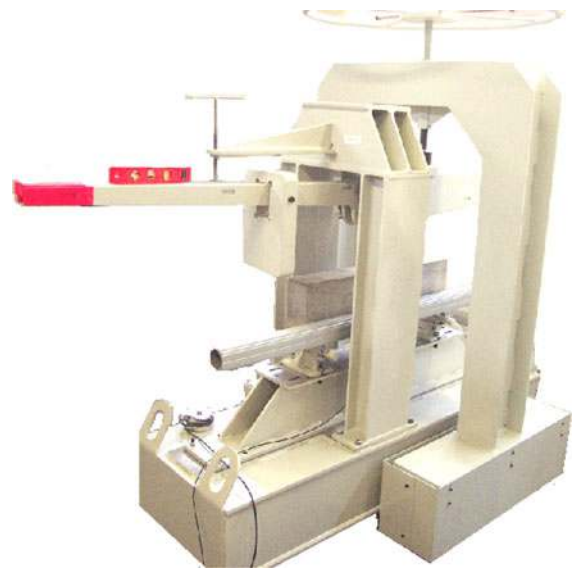

Fig. 2 General view of creep frames

40 dB gain differential amplifier. In order to overcome the background noise, the signal detection threshold was set at a value of about 30 dB (value adjusted before every test) slightly above the measured background noise [26]. The acquisition system was calibrated before each test using a pencil lead break procedure HSU-NIELSEN (Norme NF EN 1330). The acquisition parameters were set as follows: peak definition time (PDT) = 100 µs, hit definition time (HDT) = 200 µs and hit lock time (HLT) = 400 µs. The effective velocity and the attenuation of acoustic waves were also calculated. The effective velocity was assumed to be 3,800 m/s. In order to eliminate mechanical and electro-magnetic disturbances, a high pass filter with a cut-off frequency of 20 kHz, and a low-pass filter with a cut-off frequency of 400 kHz were used. Signal descriptors such as rise time, counts, energy, duration, amplitude, average frequency and counts to peak were calculated by AEwin system. Each waveform was digitized and stored. The descriptors were further analyzed and evaluated with Noesis software.

3 Mechanical results of the three-point bending tests

3.1 Results on creep tests

The experimental creep tests are presented in Fig. 3. The displacement rate is very fast in the first days of loading (primary creep) and stabilizes after a few weeks (secondary creep). In order to determine the cracking behaviour of concrete beams during their service-life, we suggest testing them at different time steps. In this study, we have chosen to stop the creep tests at 4 months. Currently, other concrete beams creep since 1 year. Results will be presented in a future paper.

The second step of this study is the characterization of creep influence on fracture properties. So a standard three-point bending test is applied.

3.2 Determination of crack properties

The purpose of this section is to investigate the effect of creep on the residual capacity of concrete specimens and the fracture energy. The beams removed from the creep frames were immediately subjected to three-point bending loading up to failure with a constant loading rate. For comparison purpose, aging specimens were tested at the same time.

Figure 4 shows the average curves of the load-CMOD for aging and creep beams. The load-CMOD variations are linear up to about 80% of the ultimate load (phase 1) followed by a nonlinear variation up to the peak load (phase 2). A stable failure was then observed and the postpeak response seems to be very gradual.

The fracture properties of concrete were also calculated. The fracture energy (G_F [N m^{-1}]) is the energy required for creating unit area of crack surface [27]. It is the ratio of the work of fracture (W_F [N m]) to the area of the uncracked ligament (A_{lig} [m^2]):

$$G_F = \frac{W_F}{A_{lig}} = \frac{W_0 + mg\delta_0}{b(d - a_0)} \quad (1)$$

W_F is divided into the work dissipated in the area under the load–deflection curve (W_0 [N m]) and the maximum displacement (δ_0 [m]) weighted by the mass of the specimen between the supports (mg [N]).

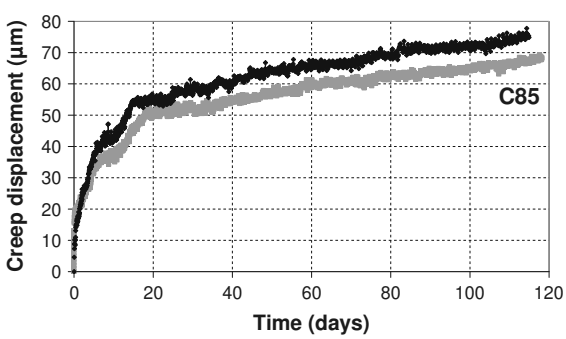

Fig. 3 Basic creep displacement of notched beams

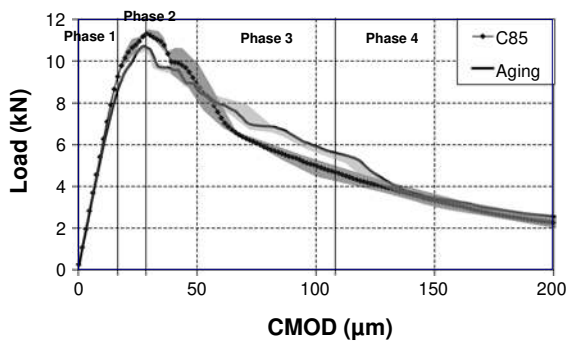

Fig. 4 Load-CMOD curves for aging and creep beams

From the load–deflection curves, the net bending stress at maximum load, or the flexural strength (f_{net}), was also calculated following the general guidelines of the RILEM 50-FMC Committee:

$$f_{net} = \frac{6(F_{max} + (mg/2))l}{4bh^2} \quad (2)$$

where h is the depth of the ligament region above the prenotch.

Results on G_F, and f_{net} are reported in Table 2 for the specimens tested at 28 days, the C85 specimens and the aging specimens. The values are the average values of two specimens. It can be seen that when specimens were subjected to creep, f_{net} tends to increase. The same observations are made for G_F. It is generally known that the fracture energy increases as strength increases [17, 23]. Thus the slight increase in energy may be explained by the strengthening effect due to basic creep [28].

Considering the measurement uncertainties, results obtained in Fig. 4 do not show distinctly the influence of creep on the fracture behaviour due to the small difference between aging and creep specimens. This small difference was also observed by Hansen [29] who reported that the fracture energy is independent of the time duration of the sustained load for three-month-old concrete specimens. The Hillerborg method seems not fine enough to assess the influence of the creep load on the fracture of concrete. Thus, the AE technique was applied to investigate micro-cracking and damage localization that takes place inside the specimens with and without creep during the three-point bending test.

4 AE analysis

Non-destructive and instrumental investigation methods such as AE technique have been conducted widely over the last years. This technique provided advance information in the exploitation and the measurement of the evolution of negative structural phenomena, such as micro- and macro-cracking that appear in the FPZ of concrete fracture [30–34]. In this work, the correlation between AE hits and load-CMOD curves of concrete beams was realised and the effect of creep on AE characteristics was studied during the three-point bending test.

Table 2 Variation of concrete fracture characteristics

	28 days	C85	Aging
G_f [N m^{-1}]	68.3 ± 0.7	85.1 ± 0.9	75.9 ± 3.8
F_{net} [MPa]	2.45 ± 0.05	2.58 ± 0	2.46 ± 0.02
F_{max} [kN]	10.75 ± 2.15	11.33 ± 0.85	10.80 ± 8.62

4.1 Localization of AE events in concrete

During the formation of a crack, energy is emitted as an elastic wave and propagates from the crack location to the AE transducers at the specimen surface. The locations of the AE sources of each event are evaluated based on the arrival times of the first wave at each transducer and their respective velocity in concrete specimen. Once the arrival time is picked, the least-square method is used to estimate the event location. A measurable event has a minimum of three well-defined arrival times.

The accuracy of the source locations was estimated by applying the pencil lead fracture at a known location on the specimens. The location resolution was estimated to be ±5 mm. This accuracy depends on many conditions such as the transducer arrangement, the covering of the herd sphere, the homogeneity of concrete, the coupling of the transducers and the variation in wave propagation velocity which may arise based on the number of aggregate crossings over the path of wave propagation and so on.

The locations of the AE sources are shown in the four stages of the fracture test (elastic stage, pre-critical crack growth, critical crack growth, cracks bridging) [35]. The cumulated locations of acoustic events throughout the tests are shown in Fig. 5a–d for aging and creep specimens. Each plotted point indicates a detected AE source. The damage accumulation is observed over a window in function of the position x and y centered at the notch, with a width of 600 mm and covering the beam depth.

4.2 Correlation of load-CMOD curve and AE parameters

In order to improve our understanding on the behaviour of aging and creep beams, several AE parameters were used during the entire loading process. AE hits provide an indication on the number of burst emissions or events, and other wave characteristics, such as the

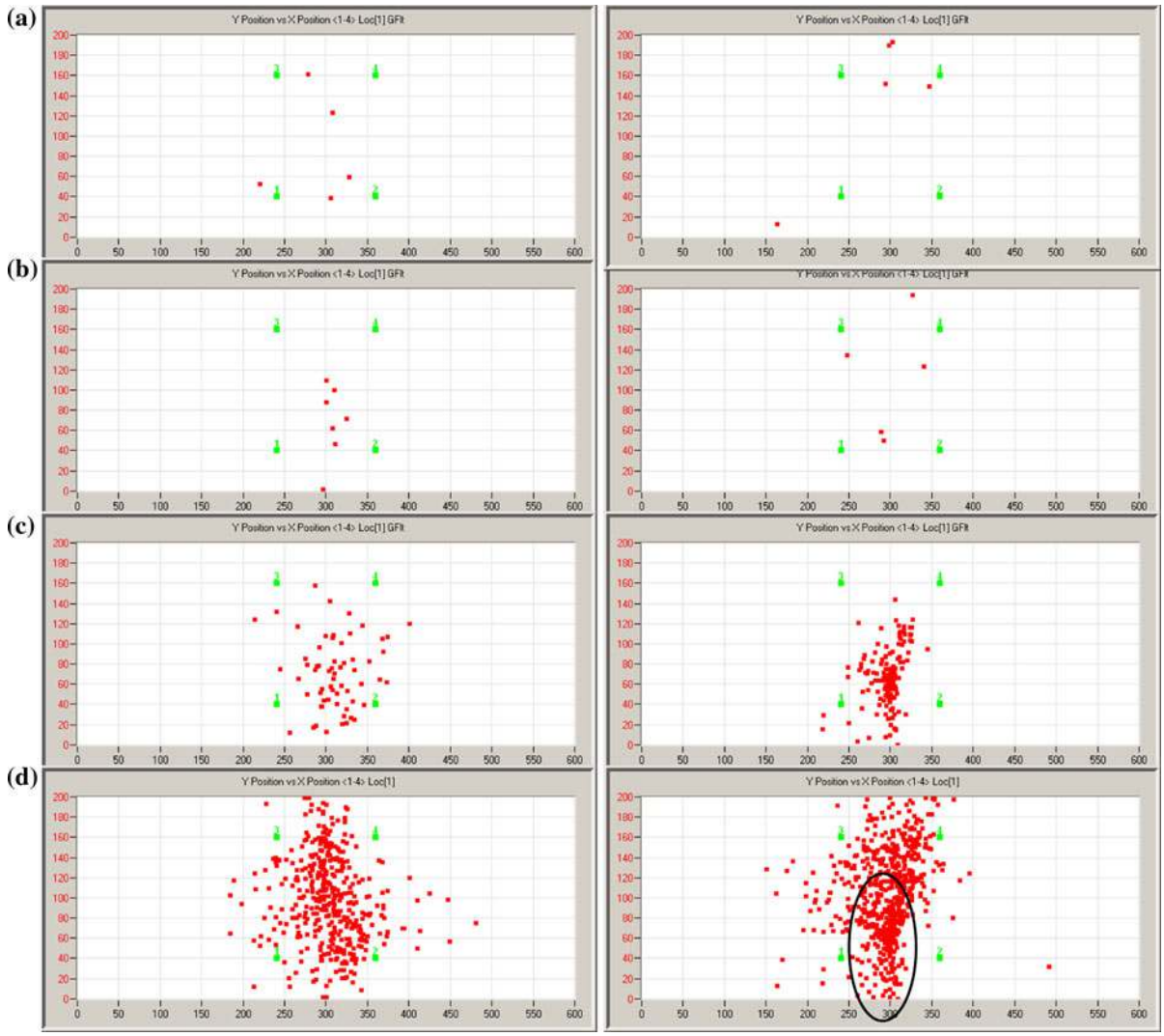

Fig. 5 Maps of the AE sources located at four stages of the loading for aging specimen (*left*) and creep specimen (*right*): **a** 0–80% of the peak load, **b** 80–100% of the peak load, **c** 100–40% of the peak load, **d** total

amplitude and the energy. The AE technique was used with all the presented specimens above. The occurrence of AE events is in a good correlation with the load-CMOD curves. In Fig. 6, the amplitude distribution (dB) is calculated as the sum of the amplitudes in any given division defined earlier as time and here the evolution of CMOD. The same results were obtained for the other two beams (Fig. 7). For clarity, the analysis of one beam in each case will be presented in the following paragraphs. The variation of AE parameters was also studied during the four stages identified earlier.

During the initial loading stage, corresponding essentially to the linear portion of the load-CMOD curve (prepeak), the AE activity was weak and few events were located; the events detected at the top of the specimen result from pressing of the rail at the beginning of the test. Micro-cracks nucleate in a somewhat random pattern in the zone of the maximum tensile stress. In addition, the amplitude and the energy of the waves released at this stage are week and thus micro-cracks occurring early in the loading cycle could be attributed to primarily matrix-aggregate interface cracks.

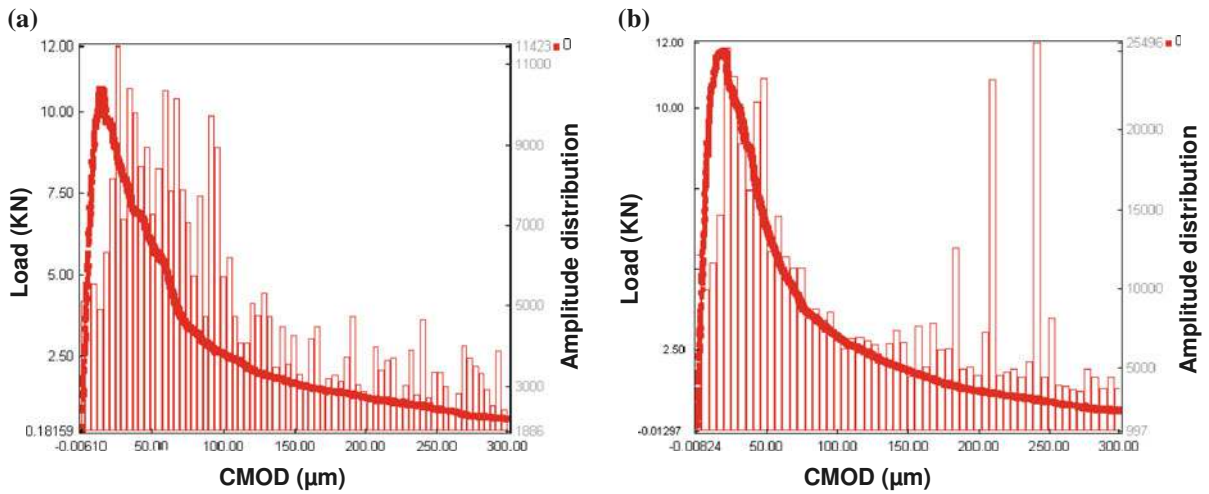

Fig. 6 Correlation of load-CMOD curve with AE amplitude distribution for aging (**a**) and creep beams (**b**)

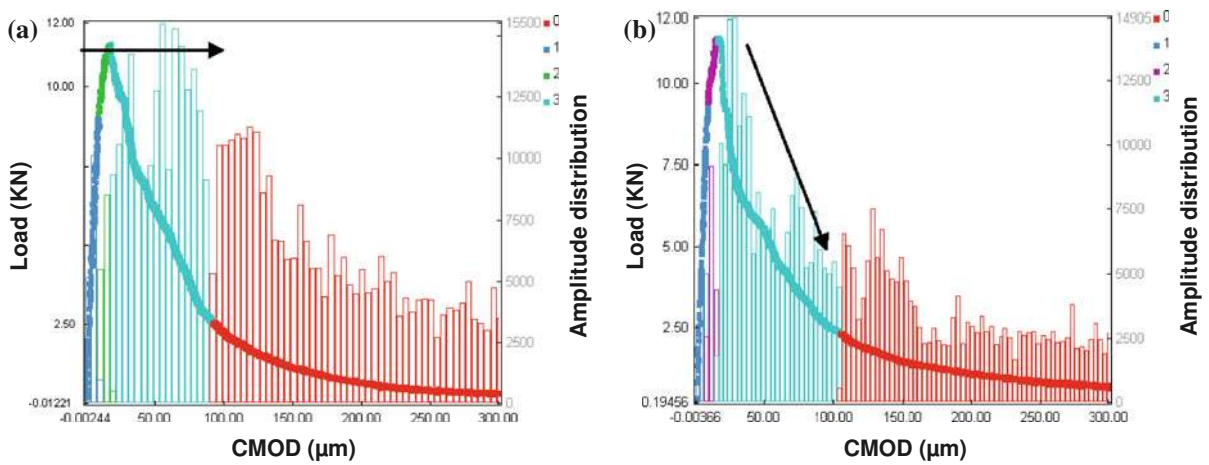

Fig. 7 Correlation of load-CMOD curve with AE amplitude distribution for aging (**a**) and creep beams (**b**) during the four phases

The second set of event locations corresponds to the prepeak nonlinear region as the load reached about 80% of the maximal strength. The AE activity became more intense indicating the formation of micro-cracks bands. In this phase, damage starts to localize around the notch tip forming the FPZ [36, 37]. As load approaches the peak, a higher energy was released indicating that there is matrix cracking around the peak load [38].

After the peak load, the AE activity increases rapidly in the third phase. This increase is associated to the high surface corresponding to cracks that develop when the external load exceeded the ultimate strength [39]. In fact at the beginning, microcracks will begin to develop at the surface of the concrete and at this point, the microcracks coalesce into an area around the location of the critical macrocracking until visible unstable cracking appears. As can be seen in Fig. 5, the locations of the AE sources increase with time and the zone becomes wider and spreading away from the notch tip. At this stage, concrete damage increases gradually with a constant AE rate.

The distinguishing characteristic that separates the initial post-peak and terminal post-peak region is the slope of the cumulative event count plot. During the terminal post-peak region, the AE activity rate decreases. This is probably due to the existing of the fracture surface inside the FPZ and the decrease of

stress [40]. AE events are generated as a consequence of different toughening mechanisms through the crack faces on micro- and meso-levels such as friction, bridgin [41].

The AE events were evenly distributed throughout the zone of maximum tensile stress in the specimen and the AE sources are localized in a band describing the way of the propagation of the crack.

4.3 Synthesis on AE results

The comparison between aging and creep specimens shows many differences. In the first stage, the AE activity was more important for aging specimen indicating the initiation of crack early in the pre-peak region (Fig. 5a). This behaviour can be also explained by the shape of the load-CMOD curve. In fact, the linear elastic phase of creep beams is more important than aging beams where the non linear behaviour begins at low loading rate. A recent study on the size effect [42, 43] showed that crack initiates at 50% in the pre-peak regime for small beams and then continues to grow gradually, while crack initiates just before the peak load for larger beams and crack length is delayed. The same behaviour is observed here with creep specimens, where the crack length is obviously delayed (Fig. 5b). Thus the behaviour of creep specimens approaches to specimen of larger size and consequently a more brittle behaviour.

The amplitude distribution shows that there existed a plateau in aging specimens and that the number of AE remains approximately constant during the third phase with no obvious occurring of AE peak distribution (Fig. 7). While the amplitude distribution for creep specimens peaked in the region of 80–90% of the maximum load in the descending branch of load-CMOD and then decreased brutally indicating a more brittle behaviour for concrete beam subjected to creep (Fig. 7). Thus, creep influences the AE characteristics and changes the distribution of hits occurring in the descending branch of the load-CMOD curves which shift to the later with aging specimen.

In addition more events were recorded with creep specimens (Fig. 5). The AE activity, proportional to the density of micro-cracking, shows a more intense localisation of micro-cracks and thus a clearer active damage zone.

Energy rate jumps were observable at certain point (Fig. 8); these discrete jumps in the energy release rate may be explained by an aggregate acting to arrest cracks before they propagate across the specimen requiring a greater driving force to propagate across the specimen [39]. The rate of the absolute AE energy decreases in the fourth phase (Fig. 8); however some AE hits present high amplitude and energy toward the end indicating different toughening mechanisms. Landis [44] suggests that the energy dissipated by fracture is proportional to the energy measured by AE technique, while the energy dissipated by toughening mechanisms do not produce a proportional response.

Figure 9 shows that the proportion of the high peak amplitude AE hits in the unstable stages is much

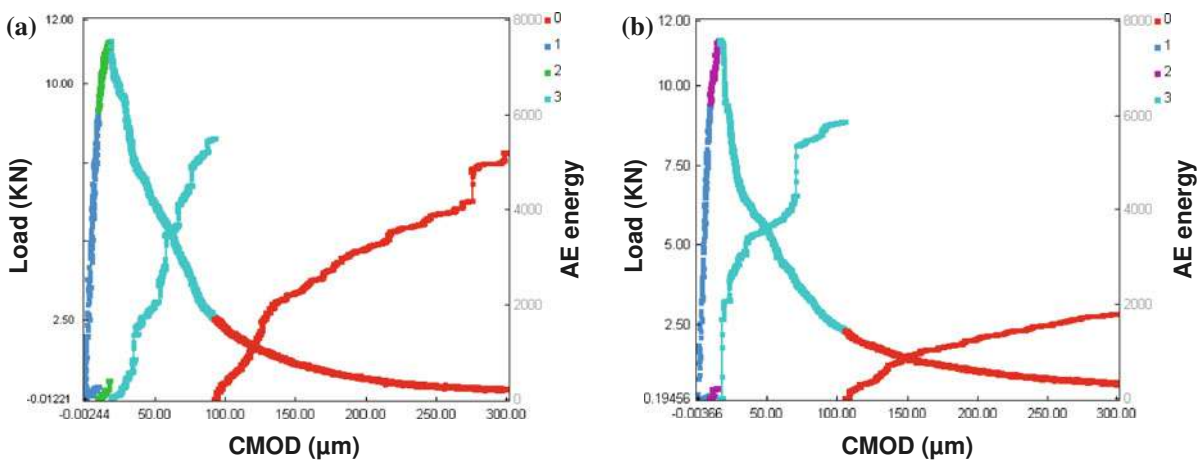

Fig. 8 Correlation of load-CMOD curve with AE energy rate for aging (**a**) and creep beams (**b**) during the four phases

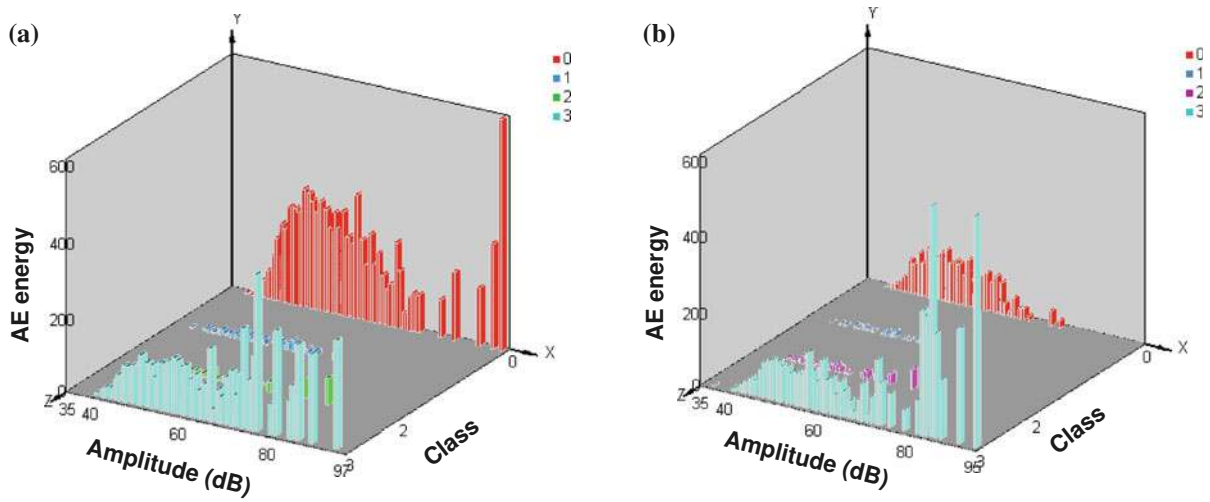

Fig. 9 Correlation between the amplitude and the acoustic energy release rate of all the waves generated for each cluster for both aging and creep beams during the four phases

higher than that in the prepeak region where the proportion of the lower peak amplitude AE hits was generally higher [32]. Thus, good correlation exists between the high peak amplitude AE hits and the growth of unstable cracks in concrete specimens.

4.4 Assessment of the FPZ width

4.4.1 Interest of the AE method to characterize the FPZ

The FPZ surrounding the crack tip is one of the principal mechanisms in the fracture of quasi-brittle materials, and nowadays is considered as the hottest topic in the field of concrete fracture mechanics. This zone is characterized by complex microstructural features in concrete in the vicinity of a macro-crack front such as frictional interlock between tortuous cracked surfaces and discontinuous fractures of unbroken aggregate bridging and other inelastic, irreversible material changes which dissipate energy [45]. This energy absorption during crack growth manifests itself in the nonlinear stress–strain behaviour and the strain softening post-peak behaviour. The size of the FPZ can be significant and depend on many parameters upon the material's microstructure: grain size, rate of loading, dimensions of the specimen [30] and other parameters such as notch depths [46].

4.4.2 Analysis of the FPZ width for concrete creep

One of the aims of the AE analysis is to compare characteristics of the FPZ for aging and creep specimens and more particularly its width. The approach used to measure the crack band width is similar to the one used by Haidar et al. [47]. This method consists of dividing the specimen into an array of rectangular elements and to count the AE events located within each element. The fineness of the grid (2×2 cm^2) was chosen large enough in order to give a sufficient number of events per element and not too small compared to the accuracy of the AE localization method. The cumulative number of events over the entire record during the experiment, is plotted as a function of its horizontal position x for various vertical positions y over the depth of the specimen at the final load step. The average curve is then presented in a continued line. The horizontal straight line which intersects the vertical axis at the value of 20% of $N_{\max}$ ($N_{\max}$ is the maximum number of events on the average curve) was plotted in the same graph (Fig. 10). The crack band width was defined arbitrarily as the length of the segment of this horizontal straight line which intersects the average distribution of AE events. This line gives us the width of the FPZ at the confidence interval by dividing the curve in two area: the first corresponding to a zone of confidence of events in which the number of AE events have higher values related to the damage of the material in front of

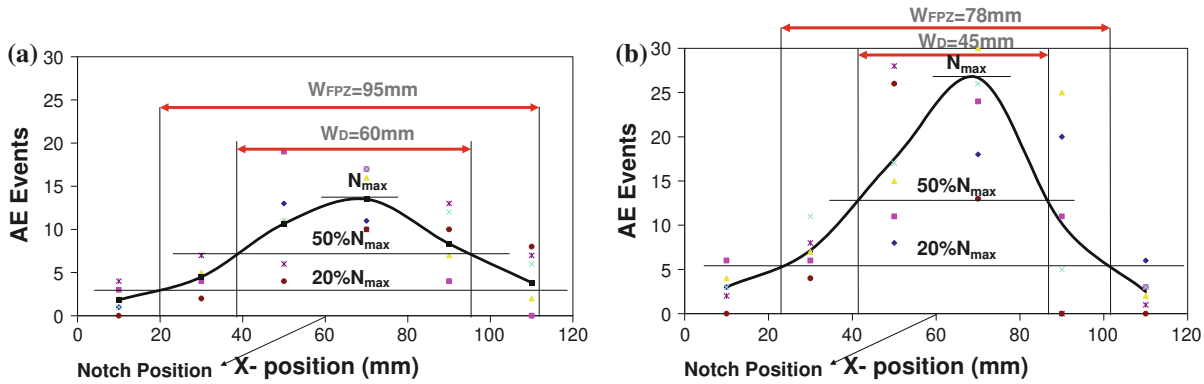

Fig. 10 Evolution of cumulative events per grid: aging specimen (**a**) and creep specimen (**b**)

the macro-crack, and the second represented by a lower percentage of AE events corresponding to lower damage [40]. The width of damage zone was also computed using the method proposed by Rossi [48]. The width of damage zone is determined by drawing a line at 50% of $N_{\max}$.

The value of the FPZ is about 95 and 78 mm and the width of the damage zone is about 60 and 45 mm for aging and creep specimens, respectively. This difference could be seen also in Fig. 5 where AE events are located into a smaller region in creep specimens. Based on these figures, the propagation of the FPZ can be also measured forward according to the loading stages [30]. This decrease of the FPZ is consistent with the results obtained by Omar [24] which show the same decrease in the size of the FPZ obtained from the size effect law and the characteristic length fitted before and after creep and thus a more brittle behaviour in the specimen.

There are several reasons for this discrepancy: on one hand, the change in the microstructure of the material under creep due to the creation of micro-cracking and defects [6], on the other hand, the consolidation of the cement paste on the compression zone during creep test. The first phenomenon is more significant in the tensile zone of the beam where tensile creep is largely a result of time-dependent microcracking [49]. As tests have been made in autogenous conditions, those microcracking may be due to the adsorption of water into the tips of preexisting or load-induced cracks, and thus more intense localization of microcracks in concrete creep beams.

A recent study conducted by Haidar showed that the width of the FPZ decreases with the porosity. Thus, the

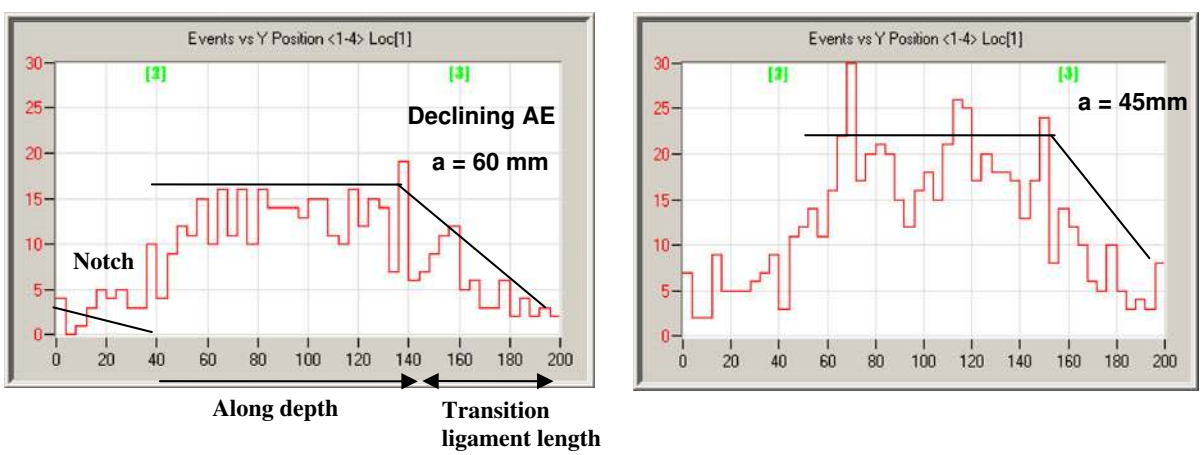

Fig. 11 Histogram of events in beam along the ligament length at the notch showing declining AE activities towards the specimen back boundary in aging specimen (*left*) and creep specimen (*right*)

shift towards a more brittle failure may be also caused by the densification and the increase of strength of the interfacial layer between the mortar matrix and the aggregate particles in the compression zone. The interface may maintain integrity in this case when a crack approaches an interfacial region and the damage process zone may be significantly reduced in size.

The same conclusion on the brittleness of creep specimens can be shown using the local fracture energy and boundary effect induced by free surface. The size effect of fracture energy through the back boundary effect is taken into account by assuming a bi-linear variation of local fracture energy over the ligament length [50–52]. The number of event occurrence, indicating the crack initiation and propagation through the beam depth, remains almost constant for some distance along the ligament length and reduces as crack propagates towards the back boundary (Fig. 11). The histogram clearly follows the energy dissipation trend shown by the boundary effect model [53]. The transition ligament length which is subsequently used to compute the real fracture energy is calculated from the AE data as the horizontal projection of the post-peak sloping portion of the histogram. It is seen that the ligament length is largest for aging specimens with $a = 60$ mm followed by creep specimens with $a = 45$ mm. This decrease of the transition ligament length indicates that the boundary influence decreases as well and thus the behaviour of creep specimens approaches to specimens of large size [54] and again a more fragile behaviour.

5 Conclusions

In this study, we have made a fine analysis on the flexural behaviour of concrete subjected to basic creep. The fracture energy and the net bending stress at the maximum load were obtained following the general guidelines of the RILEM 50-FMC Committee. The creep influence on the fracture behaviour is not significant by applying the Hillerborg method. However AE analysis yields wealth information about the fracture process and helps in the understanding of microcracking and its role in the mechanical behaviour. The results show that the AE technique could be used to observe localization phenomena in concrete specimens. The evolution of the FPZ was clearly observed from the AE source location maps. The characteristics of the AE waves show a good correlation with the tension-softening properties. The FPZ was created in front of the notch near the peak load and most of the energy is released after the peak load. The decrease of the amplitude distribution after the peak load and the decrease of the width of the FPZ zone indicate a more brittle behaviour for creep specimens.

Accordingly, we can conclude that when concrete is submitted to a sustained load, two opposing effects appear: consolidation and consequently strengthening in the compression zone, and cracking and consequently weakening in the tension zone. The relative magnitude of these effects will depend on the load level and its manner of application. More experiments will be conducted using the AE technique during flexural creep tests in order to detect any damage occurring inside the material and will be presented in a future paper.

Acknowledgment This study has been performed in the project MEFISTO which is supported by the French National Research Agency (ANR—Agence Nationale pour la Recherche) in the program “Villes Durables” (Sustainable Cities) under grant number VD08_323065.

References

1. Glanville WH, Thomas FG (1939) Further investigation on the creep or flow of concrete under load. Building Research Technical Paper, Department of Scientific and Industrial Research 21
2. Bernal JD, Megaw HD (1935) The function of hydrogen in intermolecular forces. Proc R Soc A 151:384
3. Ghosh RS (1973) A hypothesis on mechanism of maturing creep of concrete. Matériaux Constr 6(31):23–27
4. Bazant ZP, Prasannan S (1989) Solidification theory for concrete creep. I: formulation. J Eng Mech 115(8):1691–1703
5. Bazant ZP, Li Y (1997) Cohesive crack with rate-dependent opening and viscoelasticity: I. Mathematical model and scaling. Int J Fract 86:247–265
6. Rossi P, Godart N, Robert JL, Gervais JP, Bruhat D (1994) Investigation of the basic creep of concrete by acoustic emission. Mater Struct 27:510–514
7. Ngab AS, Slate FO, Nilson AH (1981) Microcracking and time-dependent strains in high strength concrete. ACI Mater J 11:262–268
8. Carrasquillo RL, Slate FO, Nilson AH (1981) Microcracking and behavior of high strength concrete subjected to short-term loading. ACI J 78(3):179–186
9. Mazzotti C, Savoia M (2002) Nonlinear creep, poisson’s ration, and creep-damage interaction of concrete in compression. ACI Mater J 99(5):450–457
10. Freudenthalt AM, Roll F (1958) Creep and creep recovery of concrete under high compressive stress. J Am Concr Inst 29(12):1111–1142

11. Meyers BL, Slate FO (1969) Relationship between time-dependent deformation and micro-cracking of plain concrete. ACI Mater J 66(1):60–68
12. Bazant ZP, Gettu R (1992) Rate effects and load relaxation in static fracture of concrete. ACI Mater J 89(5):456–468
13. Carpinteri A, Valente S, Zhou FP, Ferrara G, Melchiorri G (1997) Tensile and flexural creep rupture tests on partially-damaged concrete specimens. Mater Struct 30:269–276
14. Challamel N, Lanos C, Casandjian C (2005) Creep damage modeling for quasi-brittle materials. Eur J Mech A 24: 593–613
15. Reviron N, Benboudjema F, Torrenti JM, Nahas G, Millard A (2007) Coupling between creep and cracking in tension. FraMCos 6—6th international conference on fracture mechanics of concrete and concrete structures
16. Masuero JR, Creus GJ (1995) Crack growth initiation in concrete like materials in the presence of creep, vol 156(1–2). SMiRT conference, Stuttgart, pp 209–218
17. Rao GA, Prasad BKR (2002) Fracture energy and softening behavior of high-strength concrete. Cem Concr Res 32:247–252
18. Guinea GV, El-Sayed K, Rocco CG, Elices M, Planas J (2002) The effect of the bond between the matrix and the aggregates on the cracking mechanism and fracture parameters of concrete. Cem Concr Res 32(12):1961–1970
19. Rossello C, Elices M (2004) Frature of model concrete 1. Types of fracture and crack path. Cem Concr Res 34: 1441–1450
20. Rossello C, Elices M, Guinea GV (2006) Frature of model concrete 2.Fracture energy and characteristic length. Cem Concr Res 36:1345–1353
21. Bocca P, Crotti M (2003) Variations in the mechanical properties and temperature of concrete subjected to cyclic loads, including high loads. Mater Struct 36:40–45
22. Menou A, Mounajed G, Boussa H, Pineaud A, Carre H (2006) Residual fracture energy of cement paste, mortar and concrete subject to high temperature. Theor Appl Fract Mech 45(1):64–71
23. Zhou FP, Barr BIG, Lydon FD (1995) Fracture properties of high strength concrete with varying silica fume content and aggregates. Cem Concr Compos 25(3):543–552
24. Omar M, Loukili A, Pijaudier-cabot G, Le Pape Y (2009) Creep-damage coupled effects: experimental investigation on bending beams with various sizes. J Mater Civ Eng 21(2):65–72
25. RILEM 50-FMC Recommendation (1985) Determination of fracture energy of mortar and concrete by means of three-point bend test on notched beams. Mater Struct 18:285–290
26. RILEM TC212-ACD recommendation (2010) Acoustic emission and related NDE techniques for crack detection and damage evaluation in concrete. Mater Struct 43:1177–1181
27. Hillerborg A (1985) The theoretical basis of a method to determine the fracture energy Gf of concrete. Mater Struct 18(106):291–296
28. Shah SP, Chandra S (1970) Fracture of concrete subjected to cyclic and sustained loading. ACI Mater J 67(10):816–825
29. Hansen EA (1991) Influence of sustained load on the fracture energy and the fracture zone of concrete. In: van Mier JGM, Rots JG, Bakker A (eds) Fracture process in concrete, rock and ceramics. E&FN Spon, London, pp 829–838
30. Otsuka K, Date H (2000) Fracture process zone in concrete tension specimen. Eng Fract Mech 65:111–131
31. Mihashi H, Nomura N (1996) Correlation between characteristics of fracture process zone and tension-softening properties of concrete. Nucl Eng Des 65:359–376
32. Wu K, Chen B, Yao W (2000) Study on the AE characteristics of fracture process of mortar, concrete and steel-fiber-reinforced concrete beams. Cem Concr Res 30:1495–1500
33. Granger S, Loukili A, Pijaudier-Cabot G, Chanvillard G (2007) Experimental characterization of the self-healing of cracks in an ultra high performance cementitious material: mechanical tests and acoustic emission analysis. Cem Concr Res 37:519–527
34. Chen B, Liu J (2004) Experimental study on AE characteristics of three-point-bending concrete beams. Cem Concr Res 34:391–397
35. Van Mier JGM (2008) Framework for a generalized four-stage fracture model of cement-based materials. Eng Fract Mech 75:5072–5086
36. Landis EN, Shah SP (1995) The influence of microcracking on the mechanical behaviour of cement based materials. Cem Based Mater 2:105–118
37. Li Z, Shah SP (1994) Localization of microcracking in concrete under uniaxial tension. ACI Mater J 91(4):372–381
38. Landis EN (1999) Micro-macro fracture relationships and acoustic emissions in concrete. Constr Build Mater 13:65–72
39. Kim B, Weiss WJ (2003) Using acoustic emission to quantify damage in restrained fiber-reinforced cement mortars. Cem Concr Res 33:207–214
40. Hadjab HS, Thimus JF, Chabaat M (2007) The use of acoustic emission to investigate fracture process zone in notched concrete beams. Curr Sci 93(5):648–653
41. Shah SP, Ouyang C (1994) Fracture mechanics for failure of concrete. Annu Rev Mat Sci 24:293–320
42. Alam SY (2011) Experimental study and numerical analysis of crack opening in concrete, Doctoral thesis, Ecole Centrale de Nantes, France
43. Alam SY, Loukili A, Grondin F (2012) Monitoring crack opening displacement in concrete beams with different sizes. Eur J Environ Civ Eng (in press)
44. Landis EN, Baillon L (2002) Experiments to relate acoustic emission energy to fracture energy of concrete. J Eng Mech 128(6):698–702
45. Shah SP, Choi S (1999) Nondestructive techniques for studying fracture processes in concrete. Int J Fract 98:351–359
46. Zhang D, Wu K (1999) Fracture process zone of notched three-point-bending concrete beams. Cem Concr Res 29: 1887–1892
47. Haidar K, Pijaudier-Cabot G, Dubé JF, Loukili A (2005) Correlation between the internal length, the fracture process zone and size effect in model materials. Mater Struct 38:201–210
48. Rossi P, Robert JL, Gervais JP, Bruhat D (1990) The use of acoustic emission in fracture mechanics applied to concrete. Eng Fract Mech 35:751–763
49. Cook DJ (1972) Some aspects of the mechanism of tensile creep in concrete. ACI Mater J 69:645–649
50. Karihaloo BL, Abdalla HM, Imjai T (2003) A simple method for determining the true specific fracture energy of concrete. Mag Concr Res 55:471–481

51. Duan K, Hu X, Wittmann FH (2003) Boundary effect on concrete fracture and non-constant fracture energy distribution. Eng Fract Mech 70:2257–2268
52. Hu X, Duan K (2004) Influence of fracture process zone height on fracture energy of concrete. Cem Concr Res 34:1321–1330
53. Muralidhara S, Raghu Prasad BK, Eskandari H, Karihaloo B (2010) Fracture process zone size and true fracture energy of concrete using acoustic emission. Constr Build Mater 24:479–486
54. Duan K, Hu X, Wittmann FH (2007) Size effect on specific fracture energy of concrete. Eng Fract Mech 74:87–96